2019

Predicting strength and strain enhancement ratios of circular fiber-reinforced polymer tube confined concrete under axial compression using artificial neural networks

Qasim S. Khan
University of Engineering and Technology, qasim@uow.edu.au

M Neaz Sheikh
University of Wollongong, msheikh@uow.edu.au

Muhammad N. S Hadi
University of Wollongong, mhadi@uow.edu.au

Predicting strength and strain enhancement ratios of circular fiber-reinforced polymer tube confined concrete under axial compression using artificial neural networks

Abstract

Numerous research studies experimentally investigated the axial compressive behavior of fiber-reinforced polymer tube confined concrete cylinders in the past two decades. However, only a limited number of research studies developed stress-strain models to predict the strength and strain enhancement ratio of fiber-reinforced polymer tube confined concrete cylinders under axial compression. The available strength and strain enhancement ratio models of fiber-reinforced polymer tube confined concrete cylinders are a function of actual confinement ratio only. This study develops strength and strain enhancement ratio models for circular fiber-reinforced polymer tube confined concrete under axial compression based on artificial neural network analyses using Purelin and Tansig transfer functions. The developed strength and strain enhancement ratio models are functions of actual confinement ratio, orientation of fibers, height to diameter ratio, and axial strain in unconfined concrete at peak axial stress. The formulation and performance evaluation of the developed strength and strain enhancement ratio models are carried out using experimental investigation results of 238 circular fiber-reinforced polymer tube confined concrete under concentric axial compression compiled from a database of 599 fiber-reinforced polymer tube confined concrete specimens. The predictions of the developed strength and strain enhancement ratio models match well with the experimental investigation results of the compiled database. The developed strength and strain enhancement ratio models exhibit smaller statistical errors than the available models in the research studies for predicting the strength and strain enhancement ratios of circular fiber-reinforced polymer tube confined concrete under axial compression.

Disciplines

Engineering | Science and Technology Studies

Publication Details

Khan, Q. S., Sheikh, M. Neaz. & Hadi, M. N. S. (2019). Predicting strength and strain enhancement ratios of circular fiber-reinforced polymer tube confined concrete under axial compression using artificial neural networks. Advances in Structural Engineering: an international journal, 22 (6), 1426-1443.

Predicting Strength and Strain Enhancement Ratios of Circular FRP Tube Confined Concrete (CFFT) under Axial Compression using Artificial Neural Networks

Qasim S. Khan[1], M. Neaz Sheikh[2], Muhammad N.S. Hadi[3*]

[1] Assistant Professor, Civil Engineering Department, University of Engineering and Technology, Lahore, Pakistan

[2] Associate Professor, School of Civil, Mining and Environmental Engineering, University of Wollongong, Australia

[3*]Associate Professor, School of Civil, Mining and Environmental Engineering, University of Wollongong, Australia, Corresponding Author
Email: mhadi@uow.edu.au

Abstract

Numerous research studies experimentally investigated the axial compressive behavior of Fiber Reinforced Polymer Tube Confined Concrete (CFFT) cylinders in the last two decades. However, only a limited number of research studies developed stress-strain models to predict the strength and strain enhancement ratio of CFFT cylinders under axial compression. The available strength and strain enhancement ratio models of CFFT cylinders are a function of actual confinement ratio only. This study develops strength and strain enhancement ratio models for circular CFFT under axial compression based on Artificial Neural Network (ANN) analyses using Purelin and Tansig transfer functions. The developed strength and strain enhancement ratio models are functions of actual confinement ratio, orientation of fibers, height to diameter ratio and axial strain in unconfined concrete at peak axial stress. The formulation and performance evaluation of the developed strength and strain enhancement ratio models are carried out using experimental investigation results of 238 circular CFFT under concentric axial compression compiled from a database of 599 CFFT specimens. The predictions of the developed strength and strain enhancement ratio models match well with the experimental investigation results of the compiled database. The developed strength and strain enhancement ratio models exhibit smaller statistical errors than the available models in the

research studies for predicting the strength and strain enhancement ratios of circular CFFT under axial compression.

Keywords*:* CFFT; Artificial Neural Network; Strength enhancement ratio; Strain enhancement ratio, Errors

Introduction

The strength and ductility of steel bar reinforced concrete (RC) columns are reduced over the design life of the structure mainly due to the corrosion of the steel reinforcement. A long period of exposure of steel reinforcement in RC columns to corrosive environments reduces the strength and ductility of RC columns, which may cause the RC columns to be strengthened or retrofitted. In the last three decades, the use of Fiber Reinforced Polymer (FRP) wrapped columns was investigated to strengthen the existing deteriorated RC columns (Demers and Neale 1994; Nanni and Bradford 1995; Watanable *et al.* 1997; Lam and Teng 2002; Berthet *et al.* 2005; Teng *et al.* 2009; Pham *et al.* 2013; Teng *et al.* 2016; Jameel *et al*. 2017; Zeng *et al*. 2017; Hadi *et al*. 2018).

In the last two decades, the use of Fiber Reinforced Polymer Tube Confined Concrete (CFFT) was investigated as a potential substitute of steel RC columns in the new column construction to reduce corrosion and attain higher strength and ductility. The CFFT is cost-effective as FRP tube serves as formwork and a protective barrier against the corrosion accelerating agents, and hence reduces the maintenance costs over the design life of the structure (Lillistone and Jolly 1997; Jolly and Lillistone 1998). A number of research investigations studied the effect of geometric property (height to diameter ratio), concrete properties (compressive strength of concrete and axial strain of unconfined concrete at peak axial stress), fiber properties (modulus of elasticity of fibers, thickness of fibers, ultimate tensile strength of fibers) and FRP properties (actual confinement ratio and orientation of fibers) on the strength (confined concrete strength)

and ductility (axial strain in confined concrete at peak axial stress) of CFFT. It is noted that column geometric property, concrete and fiber properties, and FRP properties significantly influence the confined concrete strength and axial strain in confined concrete at peak axial stress of CFFT (Mirmiran *et al.* 1998; Fam and Rizkalla 2001, 2002; Hong and Kim 2004; Mohamed and Masmoudi 2008; Masmoudi and Mohamed 2011; Park *et al.* 2011; Ozbakkaloglu 2013; Ozbakkaloglu and Vincent 2013; Vincent and Ozbakkaloglu 2013; Hadi *et al.* 2016; Khan *et al.* 2016; Khan *et al*. 2017; Khan *et al*. 2018).

A comprehensive review of available literature showed that numerous stress-strain models were developed to determine the confined concrete strength and ultimate confined concrete strain of FRP wrapped concrete (Ozbakkaloglu *et al.* 2012). The available stress-strain models of FRP wrapped confined concrete overestimated the confined concrete strength and ultimate confined concrete strain of CFFT (Saafi *et al.* 1999; Toutanji 1999). The stress-strain curves of FRP wrapped and FRP tube confined concrete (CFFT) are similar (Khan *et al.* 2016). However, stress-strain behaviors of FRP wrapped and CFFT are different. This is because in FRP wrapped concrete fibers are predominantly oriented in the circumferential direction resulting in negligible longitudinal stiffness. In CFFT, fibers in FRP tube are oriented in axial and circumferential directions. The longitudinal fibers in the FRP tube provide the longitudinal stiffness of the tube. A part of circumferential strain in FRP tube comes from the longitudinal stiffness of the tube due to the Poisson effect (Lam and Teng, 2003).

A limited number of research studies developed the stress-strain models to determine the confined concrete strength and ultimate confined concrete strain of CFFT. Lam and Teng (2003), Ozbakkaloglu and Lim (2013), Lim and Ozbakkaloglu (2014) and Khan *et al.* (2016) developed strength enhancement ratio models for circular CFFT. De Lorenzis and Tepfers (2002), Ozbakkaloglu and Lim (2013), Lim and Ozbakkaloglu (2014) and Khan *et al.* (2016) developed strain enhancement ratio models for circular CFFT.

Khan *et al.* (2016) developed a stress-strain model of CFFT as a function of actual confinement ratio and confinement modulus to determine the confined concrete strength and ultimate confined concrete strain of circular CFFT with fibers oriented only along the circumferential direction under axial compression. Moreover, the model predicted the confined concrete strength and ultimate confined concrete strain of CFFT with smaller errors than the errors in the available stress-strain models of circular CFFT proposed by De Lorenzis and Tepfers (2002), Lam and Teng (2003), Ozbakkaloglu and Lim (2013) and Lim and Ozbakkaloglu (2014). However, the errors in predicting the confined concrete strength and ultimate confined concrete strain using Khan *et al*. (2016) model are still considerable as the model was developed for the CFFT with fibers oriented only along the circumferential direction. It is noted that FRP tube confinement in CFFT is dependent on the geometry of the CFFT, concrete and fiber properties and FRP properties. The actual confinement ratio ($f_{l,a}/f_{co}$) is a function of the modulus of elasticity of fibers (E_f), thickness of fibers (t_f), circumferential rupture strain of fibers (ε_{rup}), diameter of CFFT (D) and unconfined concrete strength (f_{co}). However, $f_{l,a}/f_{co}$ does not directly incorporate parameters such as the orientation of fibers, height to diameter ratio and axial strain of unconfined concrete at peak axial stress. Thus, it is necessary to improve the accuracy of stress-strain model to predict the confined concrete strength and ultimate confined concrete strain of CFFT by incorporating geometric property, concrete and fiber properties and FRP properties in addition to actual confinement ratio.

In recent years, Artificial Neural Network (ANN) analysis has been used in structural design and optimization (Pham and Hadi 2014a). The ANN is of interest to the researchers to model complex civil engineering problems which are dependent on numerous variables and interrelationships between different variables. One such complex civil engineering problem is FRP confined concrete which is dependent on numerous variables and is influenced by

interrelationships between the variables. The ANN develops interrelationships between input variables and output variables, which improves the predictions of the developed models. The ANN models are simpler, user-friendly and useful for the design engineers. Naderpour *et al.* (2010); Elsanadedy *et al.* (2012); Jalal and Ramezanianpour (2012); Pham and Hadi (2013) and Pham and Hadi (2014a, b) developed models based on ANN analysis to predict the confined concrete strength and ultimate confined concrete strain of FRP confined concrete with smaller errors. Mansouri *et al*. (2016) developed models to predict the confined concrete strength, ultimate confined concrete strain and circumferential rupture strain of FRP (FRP wrapped and FRP tube) confined concrete using artificial intelligence techniques including ANN. Mansouri *et al.* (2018) developed model to predict the peak and residual conditions (confined concrete strength and ultimate confined concrete) of actively confined concrete using artificial intelligence techniques including ANN. In this study, based on ANN analysis, strength and strain enhancement models are developed to determine the confined concrete strength and ultimate confined concrete strain of circular CFFT only as functions of actual confinement ratio, orientation of fibers, height to diameter ratio and axial strain of unconfined concrete at peak axial stress.

Experimental database

The experimental database of 238 circular CFFT adopted in this study was taken from the most comprehensive experimental database of 599 CFFT compiled from 30 different experimental investigations in Khan *et al.* (2016). The collated database includes hollow, and partially and completely filled circular and non-circular CFFT with and without reinforcements (steel or FRP) tested under concentric and eccentric axial compression, flexural, cyclic or seismic loadings. The details of the experimental database of 599 CFFT can be found in Khan *et al* (2016). The database presented in this study includes only circular CFFT tested under

127 concentric axial compression and CFFT failed at the mid-height by rupturing of fibers. The
128 experimental database of 238 circular CFFT used herein consisted of two datasets. The first
129 dataset comprised experimental investigation results of 134 circular CFFT with fibers oriented
130 only along the circumferential direction. The details of the dataset of 134 circular CFFT can be
131 found in Khan *et al.* (2016). The second dataset comprised experimental investigation results
132 of 104 circular CFFT with fibers oriented in the directions other than the circumferential
133 direction. The details of 104 circular CFFT with fibers oriented in the directions other than the
134 circumferential direction (98 out of 104 CFFT were with fibers oriented at 75° with the
135 longitudinal direction) are presented in Table 1. The experimental database of 238 circular
136 CFFT included CFFT tested under concentric axial compression only and failed due to the
137 rupture of the fibers at the mid-height of FRP tube. The collated experimental database included
138 CFFT fabricated by either filament winding technique or wet layup technique. The CFFT
139 collated from Mirmiran *et al*. (1998), Samaan *et al*. (1998), Saafi *et al*. (1999) and Li *et al*.
140 (2007) were fabricated with filament winding technique. The CFFT collated from
141 Ozbakkaloglu (2013), Ozbakkaloglu and Lim (2013), and Vincent and Ozbakkaloglu (2013a
142 and b) were fabricated with wet layup technique. The collated experimental database included
143 CFFT with fibers oriented at 45º to 90º with the longitudinal direction. In the collated CFFT
144 database, only 6 CFFT were with fibers oriented at less than 75° with the longitudinal direction
145 and 232 CFFT were with fibers oriented at 75° or higher than 75° with the longitudinal
146 direction. The experimental database provided information about type of fibers (glass fiber
147 reinforced polymer GFRP; and aramid fiber reinforced polymer AFRP), geometrical properties
148 of the CFFT (Diameter, D and height to diameter ratio, H/D), properties of concrete
149 (unconfined concrete strength, f_{co} and axial strain of unconfined concrete at peak axial stress,
150 ε_{co}), properties of fiber (thickness, t_f; modulus of elasticity, E_f; tensile strain of fibers, ε_{fu}
151 and ultimate tensile strength, f_{fu}), properties of FRP (orientation, θ; circumferential rupture

strain, ε_{rup}; actual confinement ratio, $f_{l,a}/f_{co}$ and strain reduction factor, k_ε), and the confined concrete strength and ultimate confined concrete strain (Strength enhancement ratio, f'_{cc}/f_{co} and strain enhancement ratio, $\varepsilon_{cu}/\varepsilon_{co}$).

Figure 1 presents the frequency distribution of the different input parameters of circular CFFT in the form of histograms showing the range of the input parameters. The $f_{l,a}/f_{co}$ of circular CFFT is a function of D, f_{co}, t_f, E_f and ε_{rup} (Eqn. 1).

$$\frac{f_{l,a}}{f_{co}} = \frac{2E_f t_f \varepsilon_{rup}}{D f_{co}} \tag{1}$$

The $f_{l,a}/f_{co}$ varies from 0.04 to 1.78 with 69.7% of circular CFFT are in the range of 0.04 - 0.50 (Figure 1a). The orientation of fibers (θ) of circular CFFT vary from 45° to 90° (with respect to the longitudinal direction) with 1.26% (3 out of 238) of CFFT in the range of 45º - 55º, 1.26% (3 out of 238) of CFFT in the range of 55º – 65º, 41.18% (98 out of 238) of CFFT in the range of 65° - 75° and 56.30% (134 out of 238) of CFFT in the range of 75° - 90° (Figure 1b). The height to diameter ratio (H/D) of circular CFFT varies from 2.0 to 2.85 with 97.5% (232 out of 238) of circular CFFT having H/D of 2.0 (Figure 1c). The axial strain of unconfined concrete at peak axial stress (ε_{co}) of circular CFFT vary from 0.2% to 1.38% with 45% of CFFT having ε_{co} of 0.2% (Figure 1d). The strength enhancement ratios (f'_{cc}/f_{co}) and the strain enhancement ratios ($\varepsilon_{cu}/\varepsilon_{co}$) of circular CFFT are presented in Figure 2. The f'_{cc}/f_{co} of circular CFFT vary between 1.01 and 3.87 with 51.7% and 32.8% of circular CFFT are in the ranges of 1.01 – 1.74 and 1.74 - 2.50, respectively (Figure 2a). The $\varepsilon_{cu}/\varepsilon_{co}$ of circular CFFT varies between 1.19 and 31.5 with 59.2% and 28.2% of circular CFFT, respectively, are in the ranges of 1.19 – 10 and 10 – 20 (Figure 2b). The available studies developed f'_{cc}/f_{co} and $\varepsilon_{cu}/\varepsilon_{co}$ models of circular CFFT as a function of actual confinement ratio only. To accurately

model f'_{cc}/f_{co} and $\varepsilon_{cu}/\varepsilon_{co}$ of CFFT, this study develops f'_{cc}/f_{co} and $\varepsilon_{cu}/\varepsilon_{co}$ models of CFFT using four input parameters ($f_{l,a}/f_{co}$, θ, H/D and ε_{co}) instead of one input parameter ($f_{l,a}/f_{co}$).

The Artificial Neural Network (ANN) analysis

The Artificial Neural Network (ANN) analysis is an assembly of interlinked elements (Matlab 2013). The processing ability of the ANN is dependent on the inter-unit connection strength of elements called weights. These weights are obtained by a process of learning from training datasets. A neuron is a building block of the neural network in which weights are adjusted and the output is produced. The determination of confined concrete strength and ultimate confined concrete strain of circular CFFT is a well-suited problem for ANN analysis as confined concrete strength and ultimate confined concrete strain depend on geometric properties of CFFT and properties of concrete, fibers and FRP. The ANN analysis develops the multivariable interrelationships between different CFFT variables based on the training subset which result in accurate predictions of confined concrete strength and ultimate confined concrete strain of CFFT.

In this paper, for the ANN analysis, a neural network is mapped between normalized inputs and normalized targets by loading actual confinement ratio ($f_{l,a}/f_{co}$), orientation of fibers (θ), height to diameter ratio (H/D) and axial strain of unconfined concrete at peak axial stress (ε_{co}) as input vectors and strength enhancement ratio (f'_{cc}/f_{co}) and strain enhancement ratio ($\varepsilon_{cu}/\varepsilon_{co}$) as target vectors in the Matlab (Matlab 2013). The feed-forward back propagation neural network architecture was used to develop a layered neural network between inputs and targets as shown in Figure 3. In the feed-forward back propagation neural network, information moves only in the forward direction from input layer neurons to hidden layer neurons and to

196 output layer neurons. Hornik *et al.* (1989) stated that multilayered neural networks with a
197 minimum of two layers (one hidden layer and one output layer) could perform accurate
198 universal approximations. After the network was developed, the layered feed-forward neural
199 network was configured and trained. The configuration is a process in which neural network
200 performs trials to adjust input and output ranges, network processing and weight initialization
201 settings to reduce the error between targets (experimental outputs) and the outputs.
202 The experimental database of 238 circular CFFT was used to train, validate and test the
203 developed layered feed-forward neural network architecture. Upadhyaya and Eryurek (1992)
204 proposed Eqn. 2 to calculate the minimum number of training data subset to train the neural
205 network which can be used to back-calculate the minimum number of neurons in the hidden
206 layer for optimum neural network model architecture.

$$\frac{w}{o} \le n \le \frac{w}{o}\log_2\left(\frac{w}{o}\right) \tag{2}$$

207 where w is the number of total weights, $n = 166$ is the number of training data points and o
208 is the number of outputs. It is noted that the minimum number of data points for training,
209 validation and testing of ANN depends on the number of input layers, hidden layers and output
210 layer. For the ANN with a larger number of layers, the network needs to perform more
211 computations, but may solve the complex problem more efficiently. The collated CFFT
212 database was randomly divided into training subset, validation subset and testing subset by
213 using the function Dividerand (Matlab 2013). However, the percentages of training subset,
214 validation subset and testing subset were selected. The training subset was varied from 50% to
215 80% to obtain the most efficient distribution of datasets. Based on the coefficient of
216 determination of training subset, validation subset, testing subset and All set, the training subset
217 was selected as 70%. The validation and testing subsets were selected as 15% each. The
218 training subset was used to compute the gradient and to optimize the weights and biases of the
219 neural network. The validation data subset was used to minimize the validation error of the

neural network in determining the weights and biases. The testing data subset was used to optimize the performance of the neural network.

In this ANN analysis, Levenberg Marquardt (*LM*) algorithm was used to train the layered feed-forward neural network. The *LM* algorithm is considered the most efficient back propagation method available in Matlab (Matlab 2013) for function fitting and model prediction problems using feed-forward neural network architecture (Pham and Hadi 2014a). In this study, two transfer functions, i.e., Pure Linear (Purelin) and Tan sigmoid (Tansig) were used to develop and train the neural networks. Naderpour *et al.* (2010) and Pham and Hadi (2014a) reported that ANN trained with non-linear tan sigmoid (Tansig) transfer function predicted the outputs with significantly higher accuracy than ANN trained with pure linear (Purelin) transfer function.

In this paper, for the ANN analysis, the performance of the trained layered feed-forward neural network was assessed using the Mean Square Error (MSE) and Regression performance indicators. The layered neural network was trained with increasing number of neurons in the hidden layer (started with a minimum number of neurons in the hidden layer determined using Eqn. 2) until the MSE of the trained layered feed-forward neural network was reduced to a value less than 0.05.

Mathematical formulations of developed strength and strain enhancement ratios of circular CFFT

The architecture of the developed layered feed-forward neural network models is presented in Figure 3. The output of developed layered feed-forward neural network models is obtained using inputs, targets, neural network weights and neural network biases as given in Eqns. (3 - 6).

$$y_1 = IW_{ji} \times X_i + b_1 \tag{3}$$

$$y_2 = TransferFunction\,(y_1) \tag{4}$$

$$y_3 = LW_{1j} \times y_2 + b_2 \tag{5}$$

$$y = TransferFunction\,(y_3) \tag{6}$$

where IW_{ji} is the input weight matrix to the hidden layer, X_i is the input layer matrix, LW is the layer weight matrix input to the output layer, b_1 is the bias matrix of hidden layer (Layer-1), b_2 is the bias matrix of output layer (Layer-2), y_1 is the output of Layer-1, y_3 is the output of Layer-2, y_2 is the intermediary matrix and y is the output.

It is noted that the output of developed layered feed-forward neural network is obtained using normalized inputs, normalized targets, neural network weights and neural network biases as given in Eqn. ().

$$\begin{aligned} y = \sum_1^i \left(\frac{y_{\max} - y_{\min}}{x_{i\max} - x_{i\min}} \right) w_{ij} x_i + \left(\frac{y_{\max} + y_{\min}}{2} \right) + \left(\frac{y_{\max} - y_{\min}}{2} \right) a \\ - \sum_1^i \left(\frac{y_{\max} - y_{\min}}{x_{i\max} - x_{i\min}} \right) w_{ij} x_{i\min} - \sum_1^i \left(\frac{y_{\max} + y_{\min}}{2} \right) w_{ij} \end{aligned} \tag{7}$$

where $y_{\min}$ is the normalized minimum target value, $y_{\max}$ is the normalized maximum target value, $x_{i\min}$ is the normalized minimum input value of the i^{th} input, $x_{i\max}$ is the normalized maximum input value of the i^{th} input, w_i is the weight of i^{th} input and y is the output. The Eqn 6 can be written in the simplified form as Eqn. (8).

$$y = \sum_1^i m_{ij}\ x_i + c \tag{8}$$

where,

$$m_{ij} = weightmatrix = \sum_{1}^{i}\left(\frac{y_{\max} - y_{\min}}{x_{i\max} - x_{i\min}}\right)w_{ij} \tag{9}$$

$$c = \text{int } ercept = \left(\frac{y_{\max} + y_{\min}}{2}\right) + \left(\frac{y_{\max} - y_{\min}}{2}\right)a + \sum_{1}^{i}\left(\frac{y_{\max} - y_{\min}}{x_{i\max} - x_{i\min}}\right)w_{ij}x_{i\min} - \sum_{1}^{i}\left(\frac{y_{\max} + y_{\min}}{2}\right)w_{ij} \tag{10}$$

$$a = LW_{ij} \times b_{ij} + b_2 \tag{1}$$

Developed strength enhancement ratio models of circular CFFT using ANN

The compiled experimental database of 238 circular CFFT was used to develop strength enhancement ratio models based on Purelin and Tansig transfer functions in terms of actual confinement ratio ($f_{l,a}/f_{co}$), orientation of fibers (θ), height to diameter ratio (H/D) and axial strain of unconfined concrete strain at peak axial stress (ε_{co}) to determine the strength enhancement ratio of circular CFFT.

Strength enhancement ratio model based on Purelin transfer function

The design and algorithm of the strength enhancement ratio model based on Purelin transfer function are as follows: the number of neural network layers is two, network type is feed-forward back propagation, number of neurons in input layer is 4, number of neurons in hidden layer is 9, number of neurons in output layer neuron is 1, training algorithm is LM, performance function is MSE and the transfer function in hidden and output layers is Purelin. The weight matrix (m_{ij}) and intercept (c) obtained after training ANN are given in Eqns. (12) and (13), respectively. The developed strength enhancement ratio model based on Purelin transfer function is presented in Eqn. (14).

$$m_{ij} = \begin{pmatrix} f_{l,a}/f_{co} & \theta & H/D & \varepsilon_{co} \\ 1.000 & 0.165 & 0.036 & 0.037 \end{pmatrix} \quad (12)$$

$$c = 0.072 \quad (13)$$

$$\frac{f'_{cc}}{f_{co}} = (1.000 \quad 0.165 \quad 0.036 \quad 0.037) \times \left(f_{l,a}/f_{co} \quad \theta \quad H/D \quad \varepsilon_{co}\right)^T + 0.072 \quad (14)$$

Strength enhancement ratio model based on Tansig transfer function

The design and algorithm of the strength enhancement model based on Tansig transfer function are similar to the design and algorithm of the strength enhancement ratio model based on Purlin transfer function, except that the number of neurons in hidden layer are 10 and transfer functions in the hidden and output layers are Tansig. The input weights, layer weights and bias to the hidden layer obtained after training ANN are given in Table 2. The developed strength enhancement ratio model based on Tansig transfer function is presented in Eqn. ((25).

$$\frac{f'_{cc}}{f_{co}} = Tanh\left(LW^T Tanh\left(IW_{ji}\left(f_{l,a}/f_{co} \quad \theta \quad H/D \quad \varepsilon_{co}\right)^T + b_{ij}\right) - 0.128\right) \quad (2)$$

Developed strain enhancement ratio models of circular CFFT using ANN

The compiled experimental database of 238 circular CFFT was used to develop the strain enhancement ratio models based on Purelin and Tansig transfer functions in terms of actual confinement ratio ($f_{l,a}/f_{co}$), orientation of fibers (θ), height to diameter ratio (H/D) and axial strain of unconfined concrete at peak axial stress (ε_{co}) to determine the strain enhancement ratio of circular CFFT .

Strain enhancement ratio model based on Purelin transfer function

The design and algorithm of the Purelin strain enhancement ratio model based on Purelin transfer function are as follows: the number of neural network layers is two, network type is feed-forward back propagation, number of neurons in input layer is 4, number of neurons in hidden layer is 10, number of neurons in output layer is 1, training algorithm is LM, performance function is MSE and the transfer function in hidden and output layers is Purelin. The weight matrix (m_{ij}) and intercept (c) obtained after training ANN are given in Eqns. (16) and (17), respectively. The developed strain enhancement ratio model based on Purelin transfer function is presented in Eqn. (18).

$$m_{ij} = \begin{pmatrix} f_{l,a}/f_{co} & \theta & H/D & \varepsilon_{co} \\ 1.001 & -0.036 & 0.107 & 0.004 \end{pmatrix} \tag{3}$$

$$c = 0.259 \tag{4}$$

$$\frac{\varepsilon_{cu}}{\varepsilon_{co}} = \begin{pmatrix} 1.001 & -0.036 & 0.107 & 0.004 \end{pmatrix} \times \begin{pmatrix} f_{l,a}/f_{co} & \theta & H/D & \varepsilon_{co} \end{pmatrix}^T + 0.259 \tag{5}$$

Strain enhancement ratio model based on Tansig transfer function

The design and algorithm of the strain enhancement model based on Tansig transfer function is similar to the design and algorithm of the strain enhancement ratio model based on Purelin transfer function except that number of neurons in hidden layer are 7 and transfer functions in hidden and output layers are Tansig. The input weights, layer weights and bias to the hidden layer obtained after training ANN are given in Table 3. The developed strain enhancement ratio model based on Tansig transfer function is presented in Eqn. ((69).

$$\frac{\varepsilon_{cu}}{\varepsilon_{co}} = Tanh\left(LW^T Tanh\left(IW_{ji}\left(\frac{f_{l,a}}{f_{co}} \quad \theta \quad \frac{H}{D} \quad \varepsilon_{co} \right)^T + b_{ij} \right) - 0.939 \right) \tag{69}$$

Verification of the developed strength and strain enhancement ratio models

The verification of the developed strength enhancement ratio models and strain enhancement ratio models based on Purelin and Tansig transfer functions were carried out using four statistical parameters: Average Absolute Error (AAE), Mean Square Error (MSE), Relative Standard Error of Estimate (RSEE) and Standard Deviation (SD).

$$AAE = \frac{\sum_{i=1}^{n=N}\left|\frac{\Pr e.(i) - Exp.(i)}{Exp.(i)}\right|}{N} \tag{20}$$

$$MSE = \frac{\sum_{i=1}^{n=N}\left[\frac{\Pr e(i) - Exp(i)}{Exp(i)}\right]^2}{N} \tag{7}$$

$$RSEE = \frac{\sqrt{\frac{\sum_{i=1}^{n=N}(Exp.(i) - \Pr e.(i))}{N-2}}}{\frac{\sum_{i=1}^{n} Exp.(i)}{N}} \tag{8}$$

$$SD = \sqrt{\frac{\sum_{i=1}^{n=N}\left(\frac{\Pr e.(i)}{Exp.(i)} - \frac{\Pr e.(avg.)}{Exp.(avg.)}\right)^2}{N-1}} \tag{9}$$

where, Pre (i) = Predicted i^{th} value by the developed model, *Exp.* (i) = Experimental i^{th} value, N = Total number of data points. Average Absolute Error (AAE) is a measure of the difference between predicted and experimental values. Mean Square Error (MSE) is a measure of the square of the difference between predicted and experimental values. Standard Deviation (SD) is a measure of the variation of predictions from the average value. Relative Standard Error of Estimate (RSEE) is a measure of the accuracy of the predictions made with a regression line.

To compare the developed strength enhancement ratio models based on Purelin and Tansig transfer functions of CFFT, the available strength enhancement ratio models of CFFT

315 developed in Lam and Teng (2002), Ozbakkaloglu and Lim (2013), Lim and Ozbakkaloglu
316 (2014) and Khan *et al*. (2016) were selected. Similarly, to compare the developed strain
317 enhancement ratio models based on Purelin and Tansig transfer functions of CFFT, the
318 available strain enhancement ratio models of CFFT developed in De Lorenzis and Tepfers
319 (2003), Ozbakkaloglu and Lim (2013), Lim and Ozbakkaloglu (2014) and Khan *et al.* (2016)
320 were selected.

321 **Performance of the developed strength enhancement ratio models**

322 The experimental database of 238 circular CFFT was used to assess the performance of the
323 strength enhancement ratio models of CFFT in Lam and Teng (2002), Ozbakkaloglu and Lim
324 (2013), Lim and Ozbakkaloglu (2014) and Khan *et al*. (2016) (Figure 4) and developed strength
325 enhancement ratio models based on Purelin and Tansig transfer functions (Figure 5). The
326 comparison between the experimental database results and the predictions of the available and
327 developed strength enhancement ratio models showed the improved accuracy of the developed
328 models in predicting the strength enhancement ratio of circular CFFT. Among the compared
329 strength enhancement ratio models, strength enhancement ratio model developed based on
330 Tansig transfer function achieved the largest coefficient of determination (R^2) of 0.73.

331 The errors of the compared strength enhancement ratio models were statistically verified and
332 presented in Figure 6. It is evident from Figure 6 that, the developed strength enhancement
333 ratio models based on Purelin and Tansig transfer functions exhibited smaller errors than the
334 available strength enhancement ratio models of CFFT. This is attributed to the fact that the
335 developed strength enhancement models incorporated the orientation of fibers, height to
336 diameter ratio of CFFT and axial strain of unconfined concrete at peak axial stress in addition
337 to actual confinement ratio whereas the available strength enhancement ratio models of CFFT
338 are functions of actual confinement ratio only. The available strength enhancement ratio

339 models were developed for the fibers oriented only in the circumferential direction. The AAE,
340 MSE, RSEE and SD of the developed strength enhancement ratio model based on Purelin
341 transfer function were 13.9%, 2.9%, 19.3% and 17.3%, respectively. The AAE, MSE, RSEE
342 and SD of the developed strength enhancement ratio model based on Tansig transfer function
343 were 11.8%, 2.4%, 17.2% and 15.2%, respectively. However, the developed strength
344 enhancement ratio model based on Tansig transfer function is more complicated than the
345 strength enhancement ratio model based on Purelin Transfer function.

346 The experimental database of 238 circular CFFT was used to assess the performance of the
347 available strain enhancement ratio models of CFFT developed in De Lorenzis and Tepfers
348 (2003), Ozbakkaloglu and Lim (2013), Lim and Ozbakkaloglu (2014) and Khan *et al*. (2016)
349 (Figure 7) and developed strain enhancement ratio models based on Purelin and Tansig transfer
350 functions (Figure 8). The comparison between the experimental database results, and
351 predictions of the available and developed strain enhancement ratio models exhibited the
352 improved accuracy of the developed strain enhancement ratio models in calculating the strain
353 enhancement ratio of circular CFFT. Among the presented existing and developed strain
354 enhancement ratio models, Tansig strain enhancement ratio model has achieved the largest
355 coefficient of determination (R^2) of 0.92.

356 The errors of the available and developed strain enhancement ratio models were statistically
357 verified and presented in Figure 9. It is evident from Figure 9 that the developed strain
358 enhancement ratio model based on Tansig transfer function exhibited smaller errors than the
359 available strain enhancement ratio models of CFFT. This is attributed to the fact that the
360 developed strain enhancement models incorporate orientation of fibers, height to diameter ratio
361 of CFFT and axial strain of unconfined concrete at peak axial stress in addition to actual
362 confinement ratio whereas available strain enhancement ratio models are functions of actual

confinement ratio and confinement modulus and were developed for CFFT with fibers oriented only along the circumferential direction. The AAE, MSE, RSEE and SD of the developed strain enhancement ratio model based on Purelin transfer function were 30.0%, 24.8%, 26.9% and 50.6%, respectively. The AAE, MSE, RSEE and SD of the developed strain enhancement ratio model based on Tansig transfer function were 18.3%, 7.6%, 19.4% and 27.7%, respectively. However, the strain enhancement ratio model based on Tansig transfer function is more complex than the strain enhancement ratio model based on Purelin transfer function.

Discussions

The weight matrices (m_{ij}) of the developed strength enhancement ratio models based on Purelin and Tansig transfer functions and the developed strain enhancement ratio models based on Purelin and Tansig transfer functions showed that all the input parameters influenced the confined concrete strength and ultimate confined concrete strain of circular CFFT. In this study, a large number of circular CFFT (56.3%) with fibers oriented along the circumferential direction (75º - 90º) were used to train the strength and strain enhancement ratio models based on Purelin and Tansig transfer functions. The fiber orientation along the circumferential direction (75º - 90º) resulted in a significant increase in the FRP tube confinement provided to the concrete core along the circumferential direction and comparatively smaller increase in FRP tube confinement provided to the concrete core along the longitudinal direction. The fibers oriented along the circumferential direction resulted in significant increases in the confined concrete strength and circumferential rupture strain but have a minor influence on the axial strain in confined concrete at peak axial stress (Vincent and Ozbakkaloglu 2013). This is evident by the significantly higher weight matrix corresponding to the orientation of fibers in strength enhancement ratio model based on Purelin transfer function (Eqn. 12) than strain enhancement ratio model based on Purelin transfer function (Eqn. 16).

387 The height to diameter ratio (H/D) of CFFT has a relatively smaller influence on the strength
388 and strain enhancement ratios of circular CFFT than the orientation of fibers as indicated by
389 the weight matrices of strength and strain enhancement ratio models based on Purelin transfer
390 function. Generally, in slender CFFT (H/D > 5), increased axial load resulted in the buckling
391 of the CFFT which resulted in non-uniform confinement pressure and hence reduction in both
392 confined concrete strength and ultimate confined concrete strain (Mirmiran *et al.* 1998).
393 Lillistone and Jolly (2000) reported that an increase in the slenderness of CFFT resulted in a
394 decrease in the FRP confinement. The effect of slenderness is more profound for CFFT with
395 H/D > 5. In this study, all the circular CFFT are in the range of short CFFT (H/D < 5). Most
396 of the available studies investigated the axial compressive behavior of CFFT with H/D of 2.
397 It is noted that CFFT with H/D greater than 3 were reinforced with either steel bars or FRP
398 bars. The database used for ANN analysis included circular CFFT without steel or FRP bars.
399 Hence H/D has a lower influence on the strength and strain enhancement ratios of circular
400 CFFT collated in this database.
401 The axial strain of unconfined concrete at peak axial stress (ε_{co}) of CFFT has a lower influence
402 on the strength and strain enhancement ratio models than the other input parameters. The ε_{co}
403 is a function of unconfined concrete strength (f_{co}) (Ozbakkaloglu and Lim 2013). Increased
404 unconfined concrete strain resulted in a change in the cracking pattern of concrete from micro
405 to macro level hence reduced the effectiveness of FRP confinement on the concrete core and
406 lowered the confined concrete strength and ultimate confined concrete strain of circular CFFT.
407 It can be concluded from the above discussion that the actual confinement ratio is the most
408 significant input parameter as the weight matrix corresponding to actual confinement ratio in
409 strength and strain enhancement ratio models based on Purelin transfer function is the highest.
410 The orientation of fibers, height to diameter ratio and unconfined concrete strain have a minor

411 influence on the confined concrete strength and ultimate confined concrete strain. Nonetheless,
412 the inclusion of orientation of fibers, height to diameter ratio and unconfined concrete strain in
413 the developed strength and strain enhancement ratio models based on Purelin and Tansig
414 transfer functions reduced the errors and improved the agreement between the predictions and
415 experimental confined concrete strength and strain enhancement ratios of circular CFFT.

416 It is noted that ANN is a computational model with an ability to generate function
417 approximations between inputs and targets because of its ability to learn and adapt. The ANN
418 is a very powerful tool but has a limitation in extrapolating a function. To use the developed
419 strength and strain enhancement ratios models based on Purelin and Tansig transfer functions
420 of circular CFFT developed in this study, it is mandatory that the inputs and targets of circular
421 CFFT should be within the maximum and minimum limits as given in Table 2. The developed
422 strength and strain enhancement ratio models of circular CFFT are applicable to actual
423 confinement ratios between 0.04 and 1.78, orientation of fibers between 45° and 90°, height to
424 diameter ratio between 2.0 and 2.85 and unconfined concrete strain between 0.20% and 1.38%.

425 ## Conclusions

426 In this study, the strength enhancement ratio models and strain enhancement ratio models of
427 circular CFFT are developed based on ANN analysis using Purelin and Tansig transfer
428 functions as functions of actual confinement ratio, orientation of fibers, height to diameter ratio
429 and unconfined concrete strain. A compiled database of experimental investigation results of
430 238 circular CFFT was used to train, validate and test the developed strength and strain
431 enhancement ratio models based on Purelin and Tansig transfer functions. The following
432 conclusions are drawn based on the formulation, performance and statistical comparison of the
433 developed strength and strain enhancement ratio models.

The weight matrices of the strength and strain enhancement ratio models based on Purelin and Tansig transfer functions showed that actual confinement ratio is the most significant input parameter in computing the strength and strain enhancement ratios of circular CFFT. The orientation of fibers, height to diameter ratio and axial strain of unconfined concrete at peak axial stress exhibited relatively smaller effects on the predictions of the strength and strain enhancement ratio models based on Purelin and Tansig transfer functions.

The developed strength enhancement ratio model based on Tansig transfer function exhibited smaller errors (AAE = 2.1%, MSE = 0.5%, RSEE = 2.1% and SD = 2.1%) than the strength enhancement ratio model based on Purelin transfer function in predicting the confined concrete strength of circular CFFT. The developed strain enhancement ratio model based on Tansig transfer function exhibited smaller errors (AAE = 11.7%, MSE = 17.2%, RSEE = 7.5% and SD = 22.9%) than the strain enhancement ratio model based on Purelin transfer function in predicting the ultimate confined concrete strain of circular CFFT. Training ANN models with Tansig transfer function can considerably reduce the errors in predicting the strength and strain enhancement ratios of circular CFFT compared to ANN models trained with Purelin transfer function.

Acknowledgements

The first author thanks the University of Engineering and Technology, Lahore and the University of Wollongong, Australia for funding his PhD studies. The authors thank the University of Wollongong, Australia for providing the research facilities to carry out this research.

References

Berthet, J., Ferrier, E. and Hamelin, P. (2005). "Compressive behavior of concrete externally confined by composite jackets. Part A: Experimental study." *Construction and Building Materials,* 19**,** 223-232.

Demers, M. and Neale, K. (1994). "Strengthening of concrete columns with unidirectional composite sheets." International proceedings of developments in short and medium span bridge engineering, Montreal, Quebec.

Elsanadedy, H. M., Al-Salloum, Y. A., Abbas, H. and Alsayed, S. H. (2012). "Prediction of strength parameters of FRP-confined concrete." *Composites Part B: Engineering,* 43**,** 228-239.

Fam, A. and Rizkalla, S. (2002). "Flexural Behavior of Concrete-Filled Fiber-Reinforced Polymer Circular Tubes." *Journal of Composites for Construction,* 6**,** 123-132.

Fam, A. Z. and Rizkalla, S. H. (2001). "Behavior of axially loaded concrete filled circular fiber reinforced polymer tubes." *ACI Structural Journal,* 98**,** 280-289.

Hadi, M. N. S., Khan, Q. S. and Sheikh, M. N. (2016). "Axial and flexural behavior of unreinforced and FRP bar reinforced circular concrete filled FRP tube columns." *Construction and Building Materials,* 122**,** 43-53.

Hadi, M. N. S., Algubri, A. H. M., Sheikh, M. N. and Carrigan, A. T. (2018). "Axial and flexural behaviour of circular reinforced concrete columns strengthened with reactive powder concrete jacket and fibre reinforced polymer wrapping". Construction and Building Materials, 172, 717-727.

Hong, W. K. and Kim, H. C. (2004). Behavior of concrete columns confined by carbon composites tubes. *Canadian Journal of Civil Engineering***,** 178-188.

Hornik, K., Stinchcombe, M. and White, H. (1989). "Multilayer feedforward networks are universal approximators." *Neural Networks,* 2**,** 359-366.

Jalal, M. and Ramezanianpour, A. A. (2012). "Strength enhancement modeling of concrete cylinders confined with CFRP composites using artificial neural networks." *Composites Part B: Engineering,* 43**,** 2990-3000.

Jameel, M. T., Sheikh, M. N. and Hadi, M. N. S. (2017). "Behavior of circularized and FRP wrapped hollow concrete specimens under axial compressive load". Composite Structures, 171, 538-548.

Jolly, C. K.and Lillistone, D. (1998). Concrete Filled FRP circular columns under eccentric loading. *Proc. of 7th International conference on Fiber Reinforced Composites.* University of Newcastle upon Tyne, UK: Woodhead publishing limited.

Khan, Q. S., Sheikh, M. N. and Hadi, M. N. S. (2018). "Concrete filled carbon FRP tube (CFRP-CFFT) columns with and without CFRP reinforcing bars: Axial and flexural interactions." Journal of Composites Part B: Engineering, 133.

Khan, Q. S., Sheikh, M. N. and Hadi, M. N. S. (2017). "Axial-Flexural interactions of GFRP-CFFT columns with and without reinforcing GFRP bars." *Journal of composites for construction***,** 11.

Khan, Q. S., Sheikh, M. N. and Hadi, M. N. S. (2016). "Axial compressive behavior of circular CFFT: Experimental database and design-oriented model." *Steel and Composite Structures,* 21**,** 921-947.

Lam, L. and Teng, J. (2002). "Strength Models for Fiber-Reinforced Plastic-Confined Concrete." *Journal of Structural Engineering,* 128**,** 612-623.

Lam, L. and Teng, J. (2003). "Design oriented stress-strain model for FRP confined concrete." Construction and Building Materials, 17, 471-489.

Li, Y. and Ou, (2007), "Compressive behavior and nonlinear analysis of self-sensing concrete filled FRP tubes and FRP steel Composite tubes", FRPRCS-8. Patras, Greece.

Lillistone, D. and Jolly, C. K. (1997). "Concrete filled fibre reinforced plastic circular columns." Proc. of *Composite construction-conventional and innovative conference, composite construction-Conventional and innovative.*

Lillistone, D. and Jolly, C. K. (2000). "An innovative form of reinforcement for concrete columns using advanced composites." *The Structural Engineer,* 78**,** 20-29.

Mansouri, I., Gholampour, A., Kisi, O. and Ozbakkaloglu, T. (2018). "Evaluation of peak and residual conditions of actively confined concrete using neuro-fuzzy and neural computing techniques." Neural Computing and Applications, 29(3), 873-888.

Mansouri, I., Ozbakkaloglu, T., Kisi, O. and Xie, T. (2016). "Predicting behavior of FRP confined concrete using neuro-fuzzy, neural network, multivariate adaptive regression spline and M5 model tree techniques." Materials and Strcutures, 49(10), 4319-4334.

Masmoudi, R. and Mohamed, H. (2011). "Axial behavior of slender concrete filled FRP tube columns reinforced with steel and carbon FRP bars." Proc. of *FRPRCS-10.* Florida, USA.

Matlab, M. (2013). MathWorks Matlab R2013b. R2013 b ed. University of Texas at Arlington.

Mirmiran, A., Shahawy, M., Samaan, M., EL Echary, H., Mastrapa, J. C. and Pico, O. (1998). Effect of column parameters on FRP confined concrete. *Journal of Composites for Construction,* 2**,** 175-185.

Mohamed, H. and Masmoudi, R. (2008). "Compressive behavior of reinforced concrete filled FRP tubes." *ACI-SP,* SP-257**,** 91-108.

Naderpour, H., Kheyroddin, A. and Amiri, G. G. (2010). "Prediction of FRP-confined compressive strength of concrete using artificial neural networks." *Composite Structures,* 92**,** 2817-2829.

Nanni, A. and Bradford, N. M. (1995). "FRP jacketed concrete under uniaxial compression." *Construction and Building Materials,* 9**,** 115-124.

Ozbakkaloglu, T. (2013). "Compressive behavior of concrete-filled FRP tube columns: Assessment of critical column parameters." *Engineering Structures,* 51**,** 188-199.

532 Ozbakkaloglu, T. and Lim, J. C. (2013). "Axial compressive behavior of FRP confined
533 concrete: Experimental test database and a new design oriented model." *Composites Part B:*
534 *Engineering,* 55**,** 607-634.

535 Ozbakkaloglu, T., Lim, J. C. and Vincent, T. (2012). "FRP confined concrete in circular
536 sections: Review and assessment of stress strain models." *Engineering Structures,* 49**,** 1068-
537 1088.

538 Ozbakkaloglu, T. and Vincent, T. (2013). "Axial Compressive Behavior of Circular High-
539 Strength Concrete-Filled FRP Tubes." *Journal of Composites for Construction*.

540 Park, J. H., Jo, B. W., Yoon, S. J. and Park, S. K. (2011). "Experimental investigation on the
541 structural behavior of concrete filled FRP tubes with/without steel rebar." *KSCE Journal of*
542 *Civil Engineering,* 15**,** 337-345.

543 Pham, T. and Hadi, M. (2013). "Strain Estimation of CFRP-Confined Concrete Columns Using
544 Energy Approach." *Journal of Composites for Construction,* 17**,** 04013001.

545 Pham, T. and Hadi, M. (2014a). "Predicting Stress and Strain of FRP-Confined
546 Square/Rectangular Columns Using Artificial Neural Networks." *Journal of Composites for*
547 *Construction,* 04014019.

548 Pham, T. and Hadi, M. (2014b). "Stress Prediction Model for FRP Confined Rectangular
549 Concrete Columns with Rounded Corners." *Journal of Composites for Construction,* 18**,**
550 04013019.

551 Pham, T. M., Doan, L. V. and Hadi, M. N. S. (2013). "Strengthening square reinforced concrete
552 columns by circularisation and FRP confinement." *Construction and Building Materials,* 49**,**
553 490-499.

554 Saafi, M., Toutanji, H. A. and Li, Z. (1999). "Behavior of concrete columns confined with fiber
555 reinforced polymer tubes." *ACI Materials Journal,* 96**,** 500-509.

556 Samaan, M. Mirmiran, A. and Shahawy, M. (1998), "Model of Concrete Confined by Fiber
557 Composites", Journal of Structural Engineering, 124, 1025-1031.

558 Teng, J., Jiang, T., Lam, L. and Luo, Y. (2009). "Refinement of a Design-Oriented Stress–
559 Strain Model for FRP-Confined Concrete." *Journal of Composites for Construction,* 13**,** 269-
560 278.

561 Teng, J. G., Wu, J. Y., Casalboni, S., Xiao, Q. G. and Zhao, Y. (2016). "Behavior and modeling
562 of fiber-reinforced polymer-confined concrete in elliptical columns." *Advances in Structural*
563 *Engineering*, 19 (9), 1359-1378.

564 Toutanji, H., A. (1999). "Stress-Strain characteristics of concrete columns externally confined
565 with advanced fiber composite sheets." *ACI Materials journal,* 96**,** 397-404.

566 Upadhyaya, B. R. and Eryurek, E. (1992). "Application of neural networks for sensor
567 validation and plant monitoring." *Nuclear Technology,* 97**,** 170-176.

568 Vincent, T. and Ozbakkaloglu, T. (2013a), "Influence of concrete strength and confinement
569 method on axial compressive behavior of FRP confined high and ultra-high strength concrete",
570 Composites Part B: Engineering, 50, 413-428.

571 Vincent, T. and Ozbakkaloglu, T. (2013b). "Influence of fiber orientation and specimen end
572 condition on axial compressive behavior of FRP confined concrete." *Construction and Building*
573 *Materials,* 47**,** 814-826.

574 Watanable, K., Nakamura, R., Honda, Y., Toyoshima, M., Iso, M. and Fujimaki, T. (1997).
575 Confinement effect of FRP sheet on strength and ductility of concrete cylinders under uniaxial
576 compression. *Procedings of of non metallic reinforcement for concrete structures.*
577

578 Zeng, J. J., Guo, Y. C., Gao, W. Y., Li, J. Z. and Xie, J. H. (2017). "Behavior of partially and
579 fully FRP-confined circularized square columns under axial compression." *Construction and*
580 *Building Materials*, 152, 319-332.

Table 1 Circular CFFT with fibers oriented in the directions other than the circumferential direction

Study	Fiber type	Geometric properties of CFFT		Properties of concrete		Properties of fiber				Properties of FRP				Strength and ductility capacity	
		D (mm)	$\frac{H}{D}$	f_{co} (MPa)	ε_{co} (%)	E_f (GPa)	f_{fu} (MPa)	ε_{fu} (%)	t_f	θ	ε_{rup} (%)	$\frac{f_{l,a}}{f_{co}}$	k_ε	$\frac{f'_{cc}}{f_{co}}$	$\frac{\varepsilon_{cu}}{\varepsilon_{co}}$
Mirmiran *et al*. (1998)	GFRP	152.5	2.0	30.9	0.20	69.6	1800	2.6	1.45	75	1.20	0.51	0.40	1.74	15.50
	GFRP	152.5	2.0	30.9	0.20	69.6	1800	2.6	1.45	75	1.80	0.77	0.60	1.83	16.50
	GFRP	152.5	2.0	30.9	0.20	69.6	1800	2.6	2.21	75	1.50	0.98	0.50	2.36	20.50
	GFRP	152.5	2.0	30.9	0.20	69.6	1800	2.6	2.21	75	1.20	0.78	0.40	2.13	14.50
	GFRP	152.5	2.0	30.9	0.20	69.6	1800	2.6	2.21	75	1.70	1.11	0.57	2.52	22.00
	GFRP	152.5	2.0	30.9	0.20	69.6	1800	2.6	2.97	75	1.40	1.23	0.47	2.77	22.00
	GFRP	152.5	2.0	30.9	0.20	69.6	1800	2.6	2.97	75	1.60	1.40	0.53	2.81	23.50
	GFRP	152.5	2.0	29.6	0.20	69.6	1800	2.6	1.45	75	1.80	0.81	0.60	2.27	14.50
	GFRP	152.5	2.0	29.6	0.20	69.6	1800	2.6	1.45	75	1.60	0.72	0.53	1.87	19.00
	GFRP	152.5	2.0	29.6	0.20	69.6	1800	2.6	1.45	75	1.80	0.81	0.60	2.04	19.00
	GFRP	152.5	2.0	29.6	0.20	69.6	1800	2.6	2.21	75	1.60	1.09	0.53	2.52	21.50
	GFRP	152.5	2.0	29.6	0.20	69.6	1800	2.6	2.21	75	1.90	1.30	0.63	3.14	21.50
	GFRP	152.5	2.0	29.6	0.20	69.6	1800	2.6	2.21	75	1.50	1.02	0.50	2.42	19.50
	GFRP	152.5	2.0	29.6	0.20	69.6	1800	2.6	2.97	75	1.30	1.19	0.43	2.91	23.00

Table 1 (Contd.)

Mirmiran *et al*. (1998)	GFRP	152.5	2.0	29.6	0.20	69.6	1800	2.6	2.97	75	1.90	1.74	0.63	3.87	26.50
	GFRP	152.5	2.0	29.6	0.20	69.6	1800	2.6	2.97	75	1.50	1.37	0.50	2.95	20.50
	GFRP	152.5	2.0	32.0	0.20	69.6	1800	2.6	1.45	75	1.90	0.79	0.63	1.85	17.00
	GFRP	152.5	2.0	32.0	0.20	69.6	1800	2.6	1.45	75	1.80	0.74	0.60	1.90	17.00
	GFRP	152.5	2.0	32.0	0.20	69.6	1800	2.6	2.21	75	1.50	0.95	0.50	2.42	19.00
	GFRP	152.5	2.0	32.0	0.20	69.6	1800	2.6	2.21	75	1.40	0.88	0.47	2.41	19.00
	GFRP	152.5	2.0	32.0	0.20	69.6	1800	2.6	2.97	75	1.30	1.10	0.43	2.69	21.00
	GFRP	152.5	2.0	32.0	0.20	69.6	1800	2.6	2.97	75	1.30	1.10	0.43	2.63	21.50
	GFRP	152.5	2.0	44.8	0.20	55.9	1800	3.2	1.45	75	1.90	0.45	0.63	1.41	12.50
	GFRP	152.5	2.0	44.8	0.20	55.9	1800	3.2	1.45	75	1.40	0.33	0.47	1.27	11.00
	GFRP	152.5	2.0	44.8	0.20	55.9	1800	3.2	2.21	75	1.80	0.65	0.60	1.86	14.50
	GFRP	152.5	2.0	44.8	0.20	55.9	1800	3.2	2.21	75	1.40	0.51	0.47	1.68	12.00
	GFRP	152.5	2.0	44.8	0.20	55.9	1800	3.2	2.97	75	1.50	0.73	0.50	2.33	15.00
	GFRP	152.5	2.0	44.8	0.20	55.9	1800	3.2	2.97	75	1.10	0.53	0.37	1.99	13.50
	GFRP	152.5	2.0	44.8	0.20	55.9	1800	3.2	1.45	75	0.90	0.21	0.30	1.15	6.50
	GFRP	152.5	2.0	44.8	0.20	55.9	1800	3.2	1.45	75	0.90	0.21	0.30	1.09	4.00
	GFRP	152.5	2.0	44.8	0.20	55.9	1800	3.2	2.21	75	1.10	0.40	0.37	1.55	10.50
	GFRP	152.5	2.0	44.8	0.20	55.9	1800	3.2	2.21	75	1.00	0.36	0.33	1.51	10.00

Table 1 (Contd.)

Mirmiran *et al*. (1998)	GFRP	152.5	2.0	44.8	0.20	55.9	1800	3.2	2.97	75	1.00	0.49	0.33	1.88	12.50
	GFRP	152.5	2.0	44.8	0.20	55.9	1800	3.2	2.97	75	1.20	0.58	0.40	1.90	12.50
	GFRP	152.5	2.0	44.8	0.20	55.9	1800	3.2	1.45	75	1.10	0.26	0.37	1.18	6.50
	GFRP	152.5	2.0	44.8	0.20	55.9	1800	3.2	2.21	75	1.00	0.36	0.33	1.44	8.00
	GFRP	152.5	2.0	44.8	0.20	55.9	1800	3.2	2.21	75	0.90	0.33	0.30	1.39	7.00
	GFRP	152.5	2.0	44.8	0.20	55.9	1800	3.2	2.97	75	1.00	0.49	0.33	1.98	13.00
	GFRP	152.5	2.0	44.8	0.20	55.9	1800	3.2	2.97	75	1.20	0.58	0.40	1.99	11.50
	GFRP	152.5	2.0	44.8	0.20	55.9	1800	3.2	1.45	75	0.90	0.21	0.30	1.07	5.50
	GFRP	152.5	2.0	44.8	0.20	55.9	1800	3.2	1.45	75	1.10	0.26	0.37	1.17	6.50
	GFRP	152.5	2.0	44.8	0.20	55.9	1800	3.2	2.21	75	1.00	0.36	0.33	1.46	8.00
	GFRP	152.5	2.0	44.8	0.20	55.9	1800	3.2	2.21	75	0.70	0.25	0.23	1.28	5.50
	GFRP	152.5	2.0	44.8	0.20	55.9	1800	3.2	2.97	75	0.90	0.44	0.30	1.84	9.50
	GFRP	152.5	2.0	44.8	0.20	55.9	1800	3.2	2.97	75	0.90	0.44	0.30	1.89	9.50
	GFRP	152.5	2.0	29.8	0.20	69.6	1800	2.6	0.30	75	2.10	0.19	0.81	1.03	5.00
	GFRP	152.5	2.0	29.8	0.20	69.6	1800	2.6	0.76	75	2.10	0.49	0.81	2.11	13.50
	GFRP	152.5	2.0	29.8	0.20	69.6	1800	2.6	0.76	75	1.80	0.42	0.70	2.19	15.00
	GFRP	152.5	2.0	29.8	0.20	69.6	1800	2.6	0.76	75	0.50	0.12	0.19	2.19	14.00
	GFRP	152.5	2.0	29.8	0.20	69.6	1800	2.6	1.21	75	2.00	0.74	0.77	3.14	21.50

Table 1 (Contd.)

Mirmiran *et al*. (1998)	GFRP	152.5	2.0	29.8	0.20	69.6	1800	2.6	1.21	75	2.10	0.78	0.81	3.10	19.50
	GFRP	152.5	2.0	29.8	0.20	69.6	1800	2.6	1.21	75	1.90	0.70	0.74	3.24	22.00
	GFRP	152.5	2.0	29.8	0.20	69.6	1800	2.6	1.65	75	1.60	0.81	0.62	3.76	23.50
	GFRP	152.5	2.0	29.8	0.20	69.6	1800	2.6	1.65	75	1.80	0.91	0.70	3.73	20.00
	GFRP	152.5	2.0	29.8	0.20	69.6	1800	2.6	1.65	75	1.80	0.91	0.70	3.73	19.50
	GFRP	152.5	2.0	29.8	0.20	69.6	1800	2.6	0.30	75	1.90	0.17	0.74	1.10	6.50
	GFRP	152.5	2.0	29.8	0.20	69.6	1800	2.6	0.76	75	2.10	0.49	0.81	2.11	13.50
	GFRP	152.5	2.0	29.8	0.20	69.6	1800	2.6	0.76	75	0.90	0.21	0.35	1.64	9.00
	GFRP	152.5	2.0	29.8	0.20	69.6	1800	2.6	0.76	75	1.50	0.35	0.58	1.97	15.00
	GFRP	152.5	2.0	29.8	0.20	69.6	1800	2.6	1.21	75	1.50	0.56	0.58	2.91	16.50
	GFRP	152.5	2.0	29.8	0.20	69.6	1800	2.6	1.21	75	1.90	0.70	0.74	2.96	18.00
	GFRP	152.5	2.0	29.8	0.20	69.6	1800	2.6	1.21	75	1.70	0.63	0.66	3.14	19.00
	GFRP	152.5	2.0	29.8	0.20	69.6	1800	2.6	1.65	75	1.50	0.76	0.58	3.66	18.50
	GFRP	152.5	2.0	29.8	0.20	69.6	1800	2.6	1.65	75	2.00	1.01	0.77	3.75	19.00
	GFRP	152.5	2.0	29.8	0.20	69.6	1800	2.6	1.65	75	1.60	0.81	0.62	3.72	26.00
	GFRP	152.5	2.0	31.2	0.20	69.6	1800	2.6	1.21	75	2.30	0.81	0.89	2.16	15.00
	GFRP	152.5	2.0	31.2	0.20	69.6	1800	2.6	1.21	75	2.00	0.71	0.77	2.07	15.50
	GFRP	152.5	2.0	31.2	0.20	69.6	1800	2.6	1.65	75	1.80	0.87	0.70	2.92	26.50

Table 1 (Contd.)

Mirmiran *et al*. (1998)	GFRP	152.5	2.0	31.2	0.20	69.6	1800	2.6	1.65	75	1.80	0.87	0.70	3.10	31.50
	GFRP	152.5	2.0	31.2	0.20	69.6	1800	2.6	1.21	75	2.30	0.81	0.89	2.02	15.50
	GFRP	152.5	2.0	31.2	0.20	69.6	1800	2.6	1.21	75	2.20	0.78	0.85	2.10	15.50
	GFRP	152.5	2.0	31.2	0.20	69.6	1800	2.6	1.65	75	2.00	0.97	0.77	2.95	21.50
	GFRP	152.5	2.0	31.2	0.20	69.6	1800	2.6	1.65	75	1.80	0.87	0.70	2.85	25.00
Saaman *et al*. (1998)	GFRP	152.5	2.0	30.9	0.20	69.6	2186	3.1	1.44	75	1.23	0.52	0.29	1.74	15.30
	GFRP	152.5	2.0	30.9	0.20	69.6	2186	3.1	1.44	75	1.77	0.75	0.41	1.83	16.35
	GFRP	152.5	2.0	29.6	0.20	69.6	2186	3.1	1.44	75	1.77	0.79	0.41	2.26	14.50
	GFRP	152.5	2.0	29.6	0.20	69.6	2186	3.1	1.44	75	1.56	0.69	0.36	1.87	18.80
	GFRP	152.5	2.0	29.6	0.20	69.6	2186	3.1	1.44	75	1.82	0.81	0.42	2.03	19.00
	GFRP	152.5	2.0	32.0	0.20	69.6	2186	3.1	1.44	75	1.92	0.79	0.45	1.85	17.15
	GFRP	152.5	2.0	32.0	0.20	69.6	2186	3.1	1.44	75	1.82	0.75	0.42	1.90	17.15
	GFRP	152.5	2.0	30.9	0.20	69.6	2186	3.1	2.20	75	1.49	0.97	0.35	2.36	20.35
	GFRP	152.5	2.0	30.9	0.20	69.6	2186	3.1	2.20	75	1.15	0.75	0.27	2.13	14.70
	GFRP	152.5	2.0	30.9	0.20	69.6	2186	3.1	2.20	75	1.68	1.09	0.39	2.53	22.05
	GFRP	152.5	2.0	29.6	0.20	69.6	2186	3.1	2.20	75	1.59	1.08	0.37	2.52	21.55
	GFRP	152.5	2.0	29.6	0.20	69.6	2186	3.1	2.20	75	1.88	1.27	0.44	3.14	21.40

Table 1 (Contd.)

Samaan *et al*. (1998)	GFRP	152.5	2.0	29.6	0.20	69.6	2186	3.1	2.20	75	1.49	1.01	0.35	2.42	19.60
	GFRP	152.5	2.0	32.0	0.20	69.6	2186	3.1	2.20	75	1.46	0.92	0.34	2.42	18.95
	GFRP	152.5	2.0	32.0	0.20	69.6	2186	3.1	2.20	75	1.35	0.85	0.31	2.41	18.85
	GFRP	152.5	2.0	30.9	0.20	69.6	2186	3.1	2.97	75	1.37	1.20	0.32	2.78	21.75
	GFRP	152.5	2.0	30.9	0.20	69.6	2186	3.1	2.97	75	1.55	1.36	0.36	2.81	23.45
	GFRP	152.5	2.0	29.6	0.20	69.6	2186	3.1	2.97	75	1.26	1.15	0.29	2.91	23.00
	GFRP	152.5	2.0	29.6	0.20	69.6	2186	3.1	2.97	75	1.94	1.78	0.45	3.87	26.65
	GFRP	152.5	2.0	29.6	0.20	69.6	2186	3.1	2.97	75	1.45	1.33	0.34	2.95	20.70
	GFRP	152.5	2.0	32.0	0.20	69.6	2186	3.1	2.97	75	1.30	1.10	0.30	2.69	21.10
	GFRP	152.5	2.0	32.0	0.20	69.6	2186	3.1	2.97	75	1.29	1.10	0.30	2.63	21.50
Vincent and Ozbakkaloglu (2013b)	AFRP	100	2.0	70.0	0.28	99.0	2930	3.0	0.60	45	0.54	0.09	0.18	1.01	2.25
	AFRP	100	2.0	79.5	0.30	99.0	2930	3.0	0.60	45	0.72	0.11	0.24	1.02	1.23
	AFRP	100	2.0	85.5	0.31	99.0	2930	3.0	0.60	45	0.53	0.07	0.18	1.02	1.29
	AFRP	100	2.0	80.5	0.30	99.0	2930	3.0	0.60	60	1.25	0.18	0.42	1.02	4.67
	AFRP	100	2.0	78.0	0.30	99.0	2930	3.0	0.60	60	1.89	0.29	0.64	1.01	4.93
	AFRP	100	2.0	74.0	0.29	99.0	2930	3.0	0.60	60	0.73	0.12	0.25	1.01	2.45
	AFRP	100	2.0	83.0	0.31	99.0	2930	3.0	0.60	75	0.95	0.14	0.32	1.30	4.03
	AFRP	100	2.0	83.0	0.31	99.0	2930	3.0	0.60	75	1.01	0.14	0.34	1.34	4.58
	AFRP	100	2.0	85.9	0.31	99.0	2930	3.0	0.60	75	1.38	0.19	0.47	1.37	4.77

Table 2: Input weights, layer weights and bias to the hidden layer for strength enhancement ratio model based on Tansig transfer function

Neuron	Input Weights, IW_{ji}				Layer Weights, LW^T	b_{ij}
	$f_{l,a}/f_{co}$	θ	H/D	ε_{c0}		
1	-2.650	-1.468	-0.261	-0.518	-1.237	2.218
2	-0.581	-1.813	1.111	-1.016	-0.797	2.249
3	2.694	2.003	-1.349	0.202	1.096	-0.726
4	1.916	1.402	-1.588	0.676	0.477	-0.493
5	0.240	-2.102	-0.420	0.590	-0.819	-0.226
6	1.676	-1.058	-0.432	-0.576	-1.348	0.073
7	0.694	-2.613	0.485	-1.277	1.524	1.324
8	-0.819	-0.585	1.453	-1.652	0.540	-1.451
9	0.803	-0.918	0.881	-1.884	0.457	2.220
10	-0.926	1.064	0.830	-2.273	0.078	-2.246

Table 3: Input weights, layer weights and bias to the hidden layer for strain enhancement ratio model based on Tansig transfer function

Neuron	Input Weights, IW_{ji}				Layer Weights, LW^T	b_{ij}
	$f_{l,a}/f_{co}$	θ	H/D	ε_{c0}		
1	-2.741	0.680	2.078	0.897	0.573	1.664
2	0.449	3.153	-0.331	-1.821	1.231	-0.206
3	-0.675	0.338	-1.881	-0.896	0.445	0.666
4	0.309	-0.771	0.928	-1.211	2.040	0.143
5	2.095	-2.491	-3.230	0.130	1.612	1.706
6	-3.051	-1.506	-0.178	-0.712	-0.749	-1.717
7	-0.462	2.953	-0.018	0.188	2.663	-3.937

Table 4: Maximum and minimum values of input and target parameters used to carry out ANN analysis of circular CFFT

Input Parameters	Maximum values	Minimum values
Actual Confinement Ratio, $f_{l,a}/f_{co}$	1.78	0.04
Orientation of fibers, θ (Degrees)	90	45
Height to diameter ratio, H/D	2.85	2
Unconfined concrete strain, ε_{co} (%)	1.38	0.20
Strength enhancement ratio (f_{cc}'/f_{co})	1.01	3.87
Strain enhancement ratio ($\varepsilon_{cc}'/\varepsilon_{co}$)	1.19	31.5

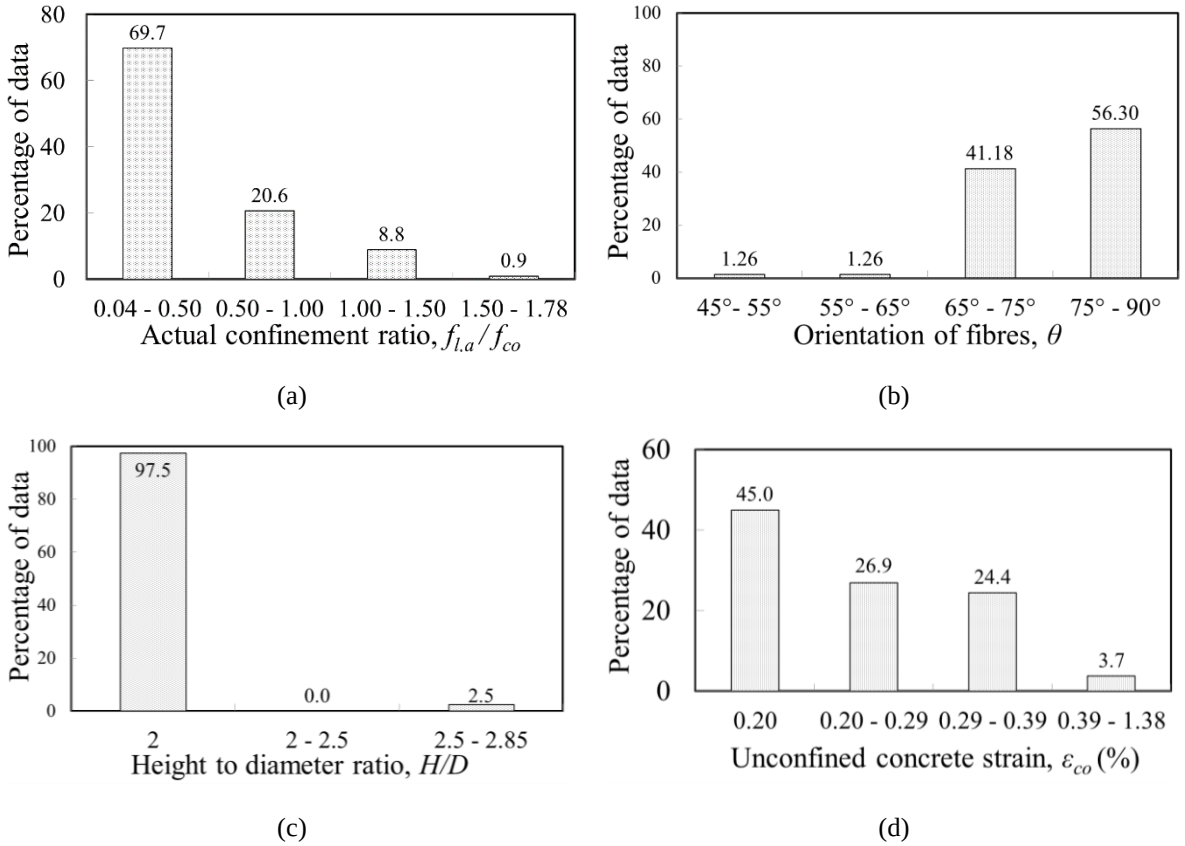

Figure 1: Frequency distribution of : (a) actual confinement ratio ($f_{l,a}/f_{co}$), (b) orientation of fibers (θ), (c) height to diameter ratio (H/D) and (d) unconfined concrete strain (ε_{co}) of circular CFFT.

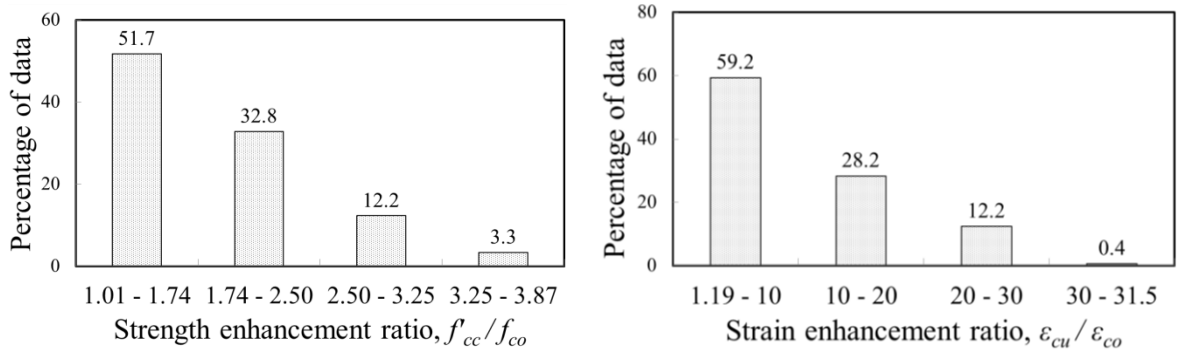

(a) (b)

Figure 2: Frequency distribution of targets: (a) strength enhancement ratio (f'_{cc}/f_{co}) and (b) strain enhancement ratio ($\varepsilon_{cu}/\varepsilon_{co}$) of circular CFFT

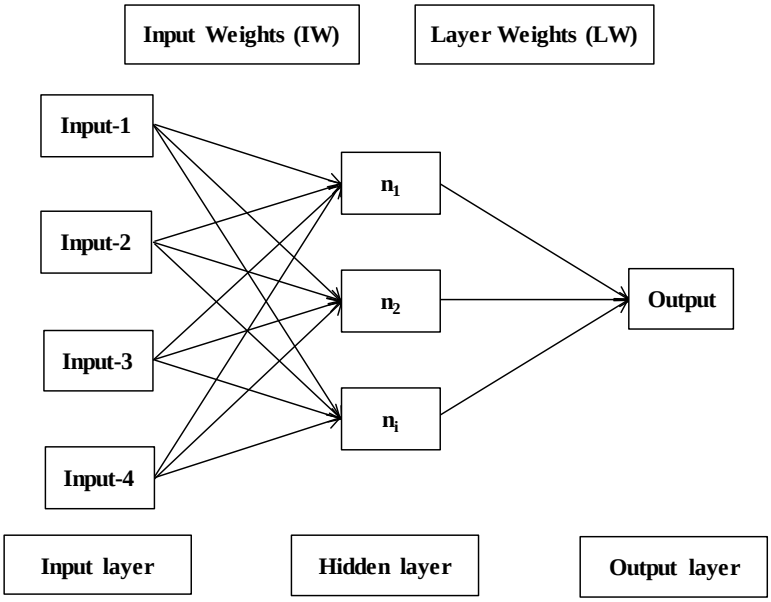

Figure 3: A schematic representation of feed forward two layered neural networks

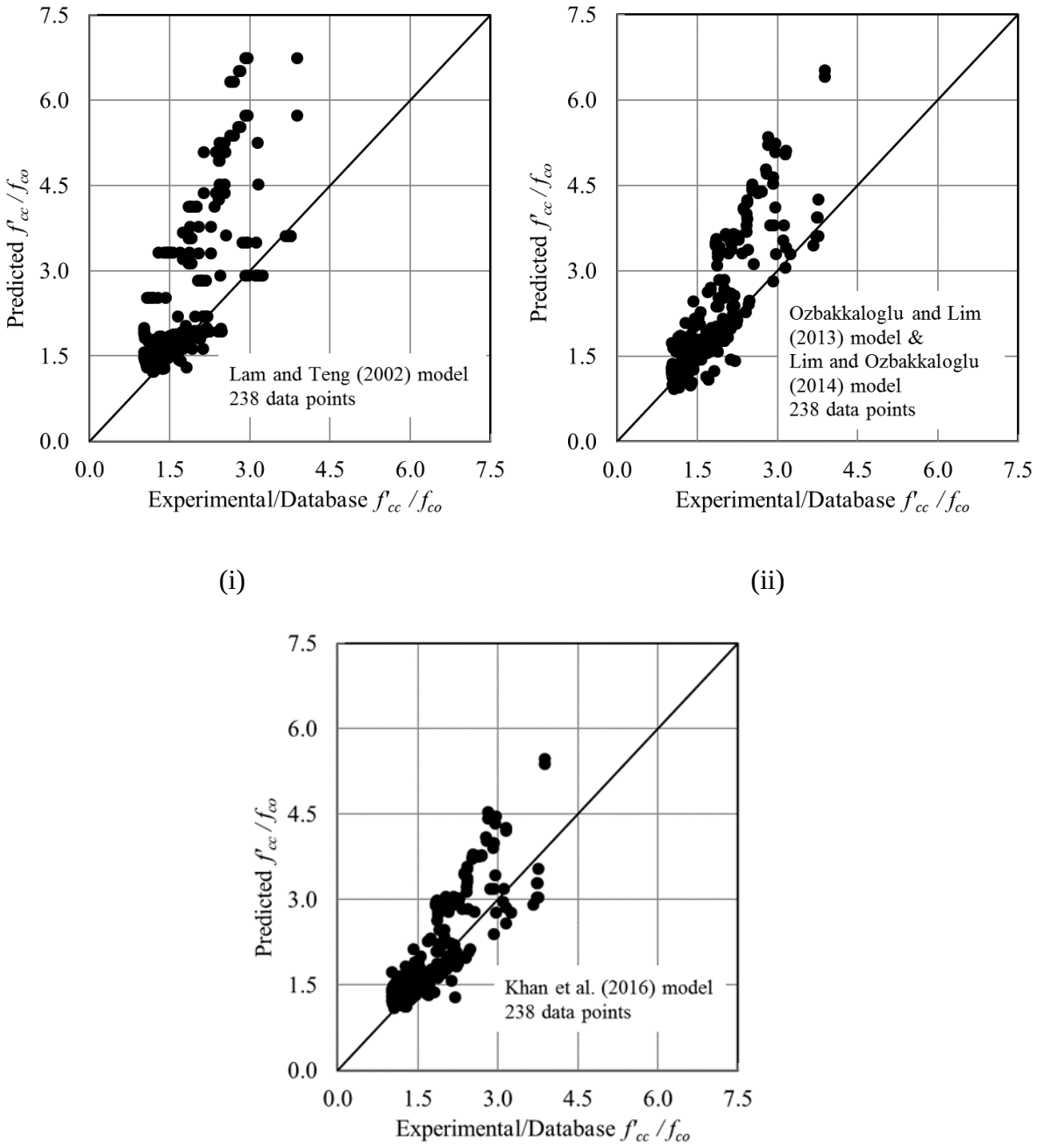

Figure 4: Performance of available strength enhancement ratio models of CFFT: (i) Lam and Teng (2002) , (ii) Ozbakkaloglu and Lim (2013) and Lim and Ozbakkaloglu (2014) and (iii) Khan *et al*. (2016)

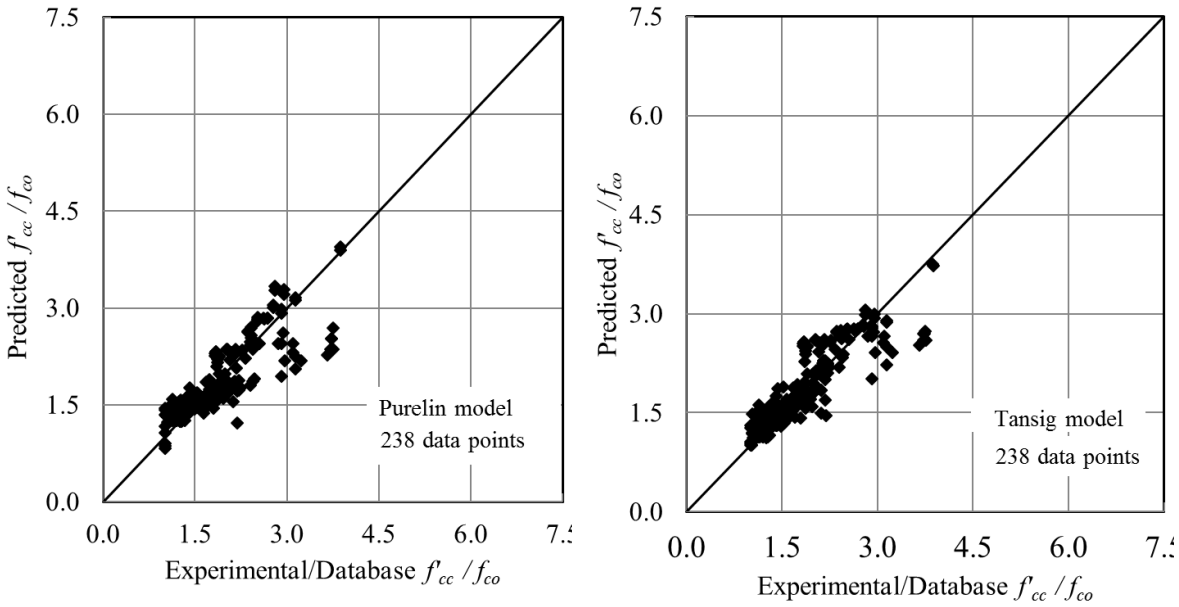

(i) (ii)

Figure 5: Performance of the developed strength enhancement ratio models based on: (i) Purelin transfer function and (ii) Tansig transfer function

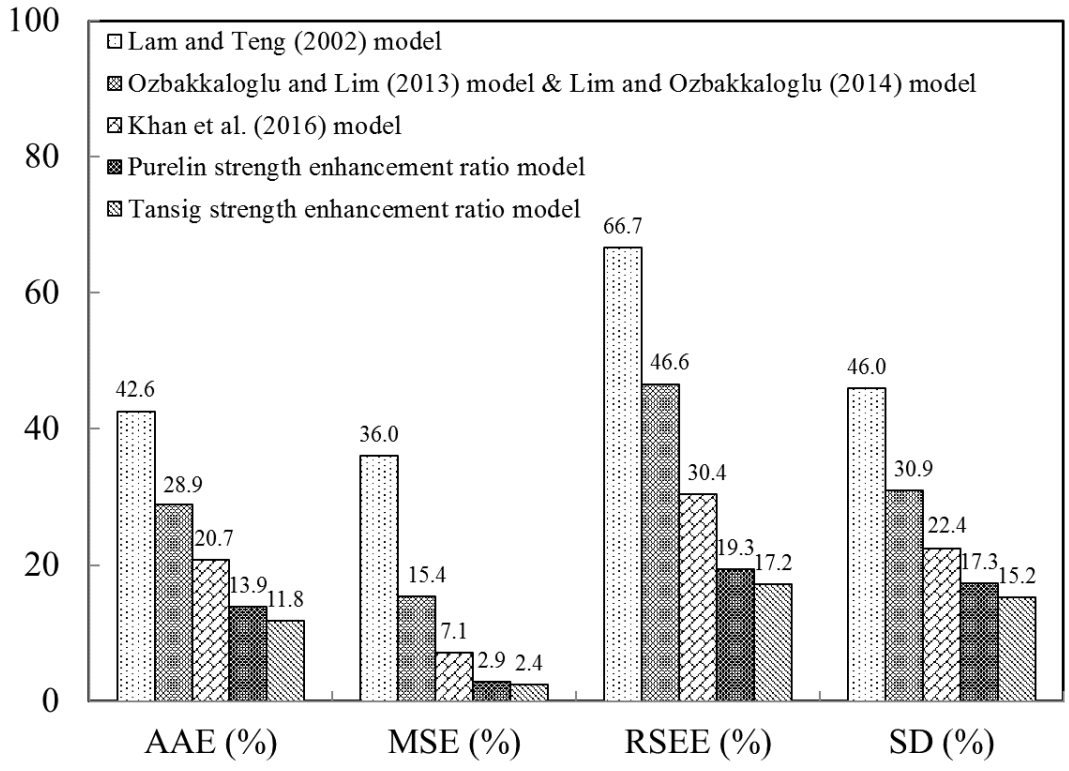

Figure 6: Statistical comparison of strength enhancement ratio models of circular CFFT

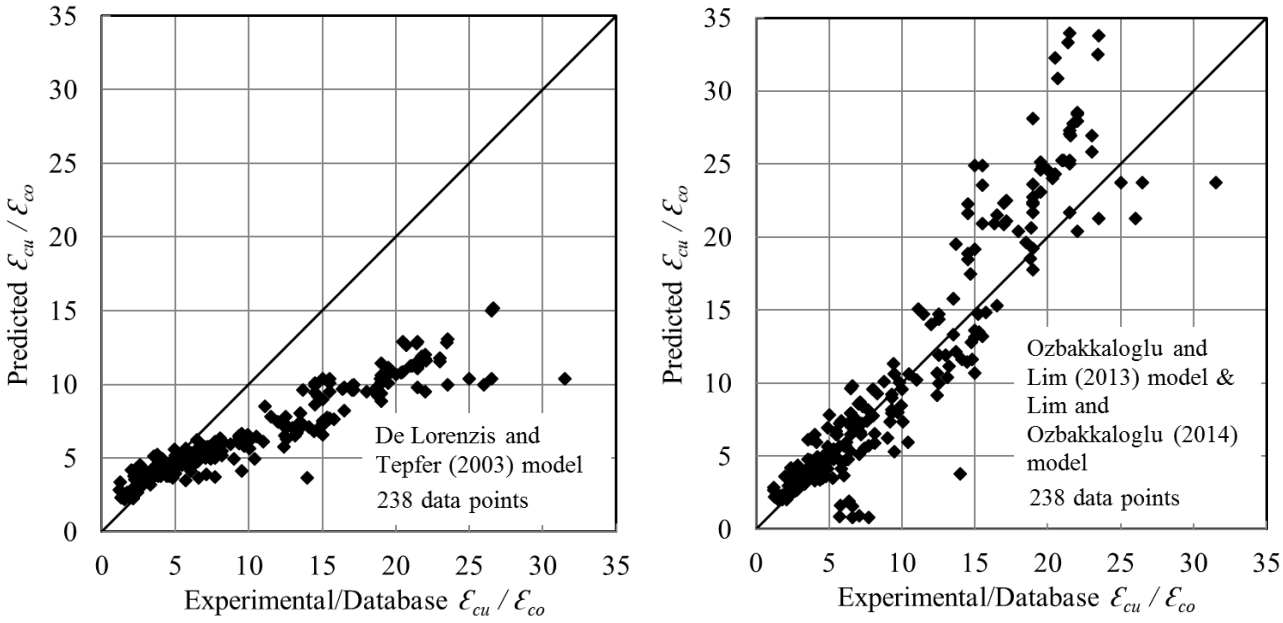

(i) (ii)

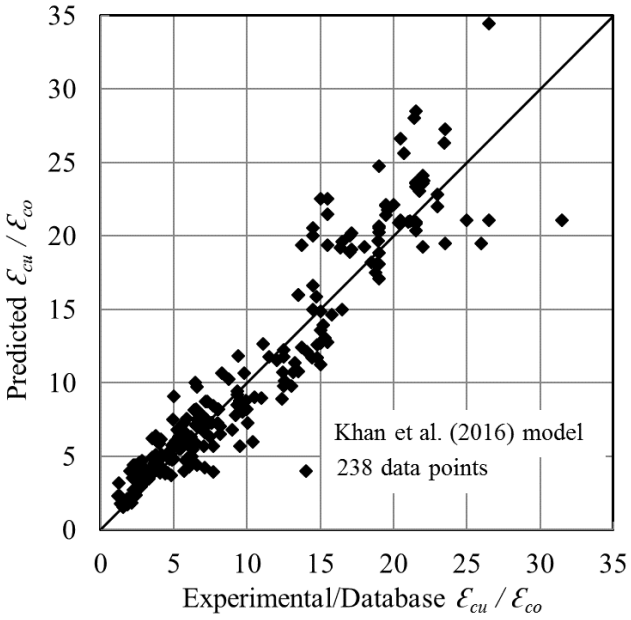

(iii)

Figure 7 : Performance of available strain enhancement ratio models: (i) De Lorenzis and Tepfers (2003), (ii) Ozbakkaloglu and Lim (2013) and Lim and Ozbakkaloglu (2014), and (iii) Khan *et al*. (2016)

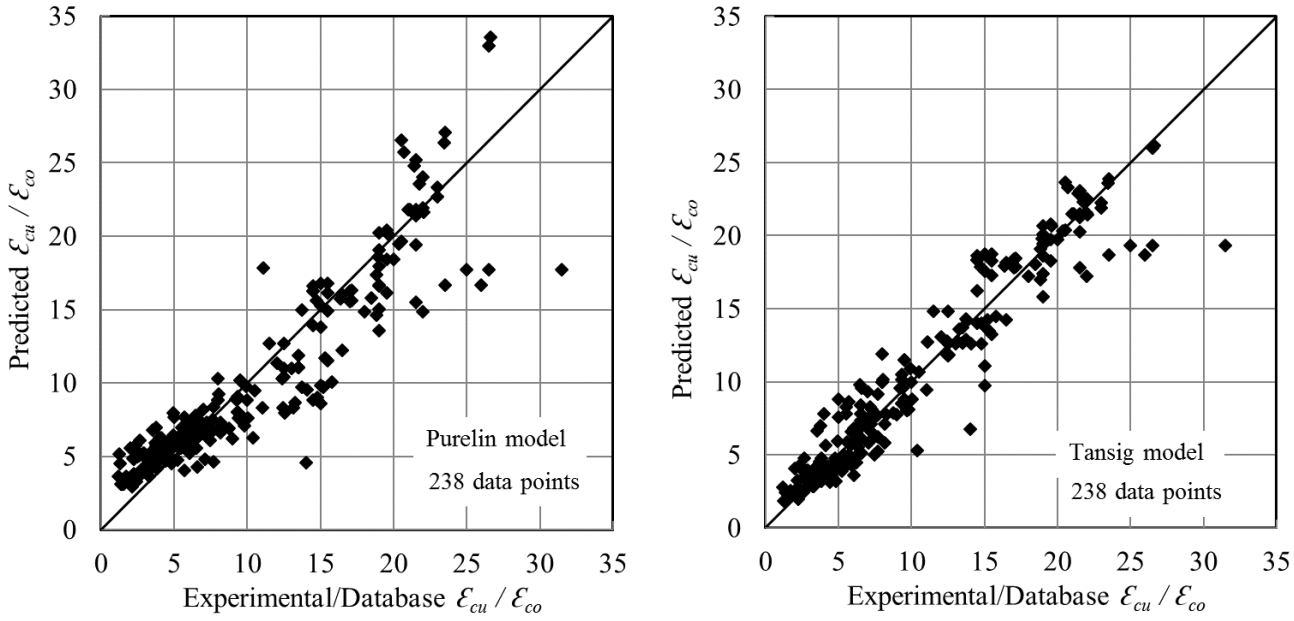

(i) (ii)

Figure 8 : Performance of the developed strain enhancement ratio models of circular CFFT based on: (i) Purelin transfer function and (ii) Tansig transfer function

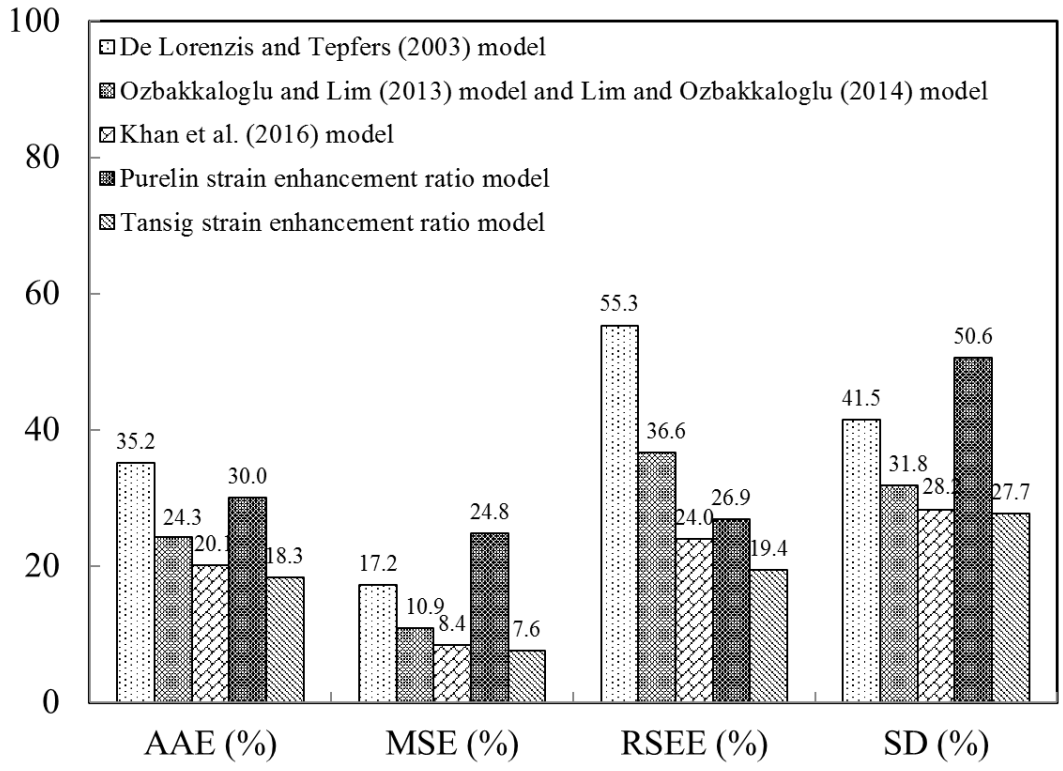

Figure 9 : Statistical comparison of strain enhancement ratio models of circular CFFT